NANO LETTERS

pubs.acs.org/NanoLett Letter

Designing Mesoporous Photonic Structures for High-Performance Passive Daytime Radiative Cooling

Meijie Chen, Dan Pang, Jyotirmoy Mandal, Xingyu Chen, Hongjie Yan, Yurong He, Nanfang Yu, and Yuan Yang*

Cite This: https://dx.doi.org/10.1021/acs.nanolett.0c04241 Read Online

ACCESS | Metrics & More | Article Recommendations | Supporting Information

ABSTRACT: Passive daytime radiative cooling (PDRC) has drawn significant attention recently for electricity-free cooling. Porous polymers are attractive for PDRC since they have excellent performance and scalability. A fundamental question remaining is how PDRC performance depends on pore properties (e.g., radius, porosity), which is critical to guiding future structure designs. In this work, optical simulations are carried out to answer this question, and effects of pore size, porosity, and thickness are studied. We find that mixed nanopores (e.g., radii of 100 and 200 nm) have a much higher solar reflectance $\bar{R}_{solar}$ (0.951) than the single-sized pores (0.811) at a thickness of 300 μm. With an Al substrate underneath, $\bar{R}_{solar}$, thermal emittance $\bar{\varepsilon}_{LWIR}$, and net cooling power P_{cool} reach 0.980, 0.984, and 72 W/m^2, respectively, under a semihumid atmospheric condition. These simulation results provide a guide for designing high-performance porous coating for PDRC applications.

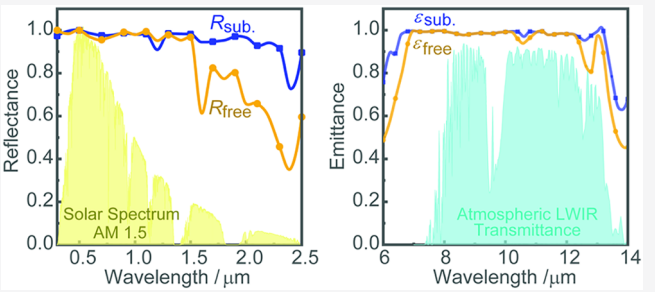

KEYWORDS: *radiative cooling, porous polymer, optical simulation, metamaterials*

INTRODUCTION

Cooling and refrigeration are becoming increasingly important for human society due to climate change, industrial development, and the improvement of living standards.[1] Current mainstream electricity-powered compression-based technologies are energy consuming and generate greenhouse and/or ozone-depleting gases.[2] They also have a net heating effect, since heat is not lost outside the terrestrial environment and the work used is ultimately dissipated as heat too.[3] Therefore, new cooling technologies without using any work are highly attractive and are urgently needed for addressing imminent challenges in climate changes.[4−6]

Passive daytime radiative cooling (PDRC) has drawn much attention recently since it is electricity-free and environmentally benign.[7−9] Unlike traditional cooling technologies that transfer heat to the surrounding (e.g., local atmosphere and cooling water), PDRC technologies move excessive heat directly to the cold outer space at ∼3 K through thermal radiation without any energy consumption.[10−12] In PDRC, a coating is designed to have a high solar reflectance $\bar{R}_{solar}$ in the wavelength (λ) of 0.3−2.5 μm to minimize sunlight absorption. It also has a high thermal emittance in the atmosphere's long-wave infrared transmission window ($\bar{\varepsilon}_{LWIR}$, $\lambda \sim 8-13$ μm) to enhance thermal radiation to the cold sky.[13] $\bar{R}_{solar}$ and $\bar{\varepsilon}_{LWIR}$ are defined as

$$\bar{R}_{solar} = \frac{\int_{0.3\mu m}^{2.5\mu m} I_{solar}(\lambda) R(\lambda)\, d\lambda}{\int_{0.3\mu m}^{2.5\mu m} I_{solar}(\lambda)\, d\lambda},$$

$$\bar{\varepsilon}_{LWIR} = \frac{\int_{8\mu m}^{13\mu m} I_{bb}(T, \lambda)\varepsilon(T, \lambda)\, d\lambda}{\int_{8\mu m}^{13\mu m} I_{bb}(T, \lambda)\, d\lambda}$$

where $I_{solar}(\lambda)$ represents the ASTM G173-03 solar spectrum at AM 1.5, $R(\lambda)$ is the spectral reflectance of coating, $I_{bb}(T, \lambda)$ is the spectral intensity emitted by a standard blackbody with a temperature of T, and $\varepsilon(T, \lambda)$ represents the sample's spectral emittance. Hence, if $\bar{R}_{solar}$ and $\bar{\varepsilon}_{LWIR}$ are high enough, even in daytime, the energy lost to the cold sky is substantially larger than heating by sunlight. Thus, electricity-free, spontaneous subambient cooling can be achieved.[14−16] Subambient cooling typically requires $\bar{R}_{solar}$ to be >0.95, or at least >0.9. On the other side, $\bar{\varepsilon}_{LWIR}$ should be over 0.7 and preferably above 0.9.[17−19]

Received: October 23, 2020
Revised: January 26, 2021

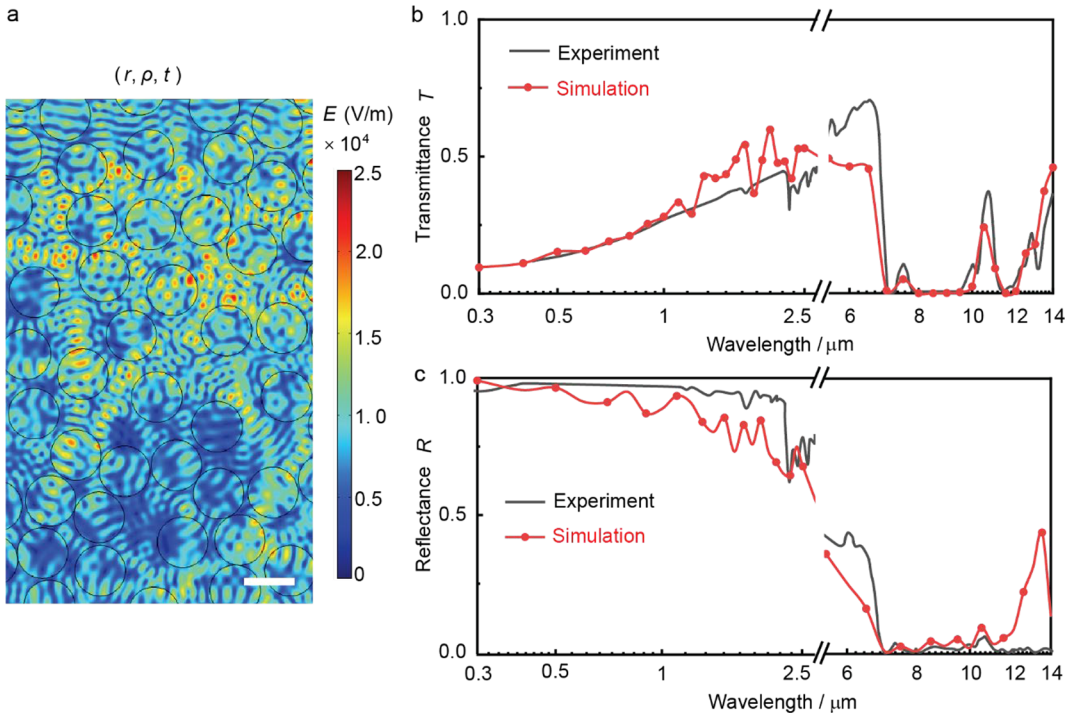

Figure 1. Validation of the simulation model for porous P(VdF-HFP) coatings. (a) The geometry of a porous structure in simulation with the electric field distribution (scale bar = 2 μm). Experimental (b) transmittance and (c) reflectance spectra[20] together with simulated spectra [(b) thickness = 93 μm; (c) thickness = 300 μm; λ = 0.3−14 μm].

Recently, porous polymer-based radiative cooling coatings, such as nano/microporous P(VdF-HFP),[20,22,23] nanoporous PE/PEO,[24−26] and cellulose-based materials,[27] have gained increasing interest owing to their potential for mass production, their low cost, and their lightweight nature.[20,21] Bulk polymers typically have low solar absorption and high thermal emittance.[28] Hence, once they are made into a mesoporous structure, where the mismatch in refractive indices between air and polymer amplifies light scattering, leading to high $\bar{R}_{solar}$ and $\bar{\varepsilon}_{LWIR}$. Among these materials, P(VdF-HFP) is attractive due to its excellent stability against ultraviolet light, making it durable for long-term outdoor applications.[29] While we have demonstrated a high $\bar{R}_{solar}$ of 0.96 ± 0.03 and $\bar{\varepsilon}_{LWIR}$ of 0.97 ± 0.02 in porous P(VdF-HFP) with bimodal hierarchical mesopores (2.7 ± 0.7 μm and 0.1 ± 0.09 μm),[20] it is unclear what the optimal pore radius distribution and porosity are. The answer is critical to engineering and optimizing mesoporous polymers for PDRC applications. Such question has not been explored in the literature, to the best of the authors' knowledge.

In this work, we build a numerical simulation model to better understand the relationship between optical properties, cooling performance, and the geometry of the porous coating, such as radius r, porosity ρ, and thickness t. P(VdF-HFP) is used as an example since its optical properties have been extensively studied.[20] Results show that when single-size pores are used, the optimal r and ρ are 0.2 μm and 0.5, respectively, for PDRC. $\bar{R}_{solar}$ and $\bar{\varepsilon}_{LWIR}$ reach 0.811 and 0.970, respectively, at a thickness of 300 μm. Mixing pores with different radii enhances the cooling performance by substantially increasing $\bar{R}_{solar}$. For example, by mixing nanopores with an r value of 0.1 and 0.2 μm, $\bar{R}_{solar}$ increases to 0.951 at t = 300 μm compared to 0.811 with single-size pores as mentioned above. These results indicate that the rational design of pore parameters is critical to enhancing PDRC performance, and this work provides a guide for optimal pore geometries.

RESULTS AND DISCUSSIONS

Model Description, Simplification, and Verification. Direct 3D simulation of porous polymers is extremely expensive due to its nonrepeatable nature. For example, with a volume of 10 × 10 × 100 μm^3 and a mesh size of ∼10 nm, the mesh number reaches a scale of tens of billions, which is very challenging to solve. To reduce the computational load, a 2D porous structure is used (Figure 1a) where round pores are randomly placed inside a rectangular slab with a target porosity (Figure S1). The 2D simulation is expected to capture key features in 3D light scattering, since individual 2D and 3D pores show a similar scattering efficiency as a function of pore radius at different wavelengths, suggesting that the optimal pore sizes for $\bar{R}_{solar}$, $\bar{\varepsilon}_{LWIR}$, and radiative cooling should be similar in 2D and 3D (see Figure S2 for details).

In 2D simulations, a full electromagnetic field calculation is performed by finite element methods (FEM) in COMSOL for obtaining reflectance ($R(\lambda)$), transmission ($T(\lambda)$), and absorptance ($A(\lambda)$). Then, $R(\lambda)$ and $A(\lambda)$ are used to calculate $\bar{R}_{solar}$ and $\bar{\varepsilon}_{LWIR}$, respectively, as conservative estimations, since the simulated porous structure is not on any substrate and common substrates (e.g., metals and concretes) further enhance $\bar{R}_{solar}$ and $\bar{\varepsilon}_{LWIR}$. Such computationally expensive FEM simulation is necessary for the solar spectrum since the pore size is comparable with the wavelengths, which leads to strong scattering at the pore/P(VdF-HFP) interface, and cannot be captured by simpler models (e.g., effective medium model/EMM) (Figure S3a). In mid-infrared wavelengths, EMM shows a good agreement with FEM as the pore size is much smaller than the wavelength (Figure S3b).

https://dx.doi.org/10.1021/acs.nanolett.0c04241
Nano Lett. XXXX, XXX, XXX−XXX

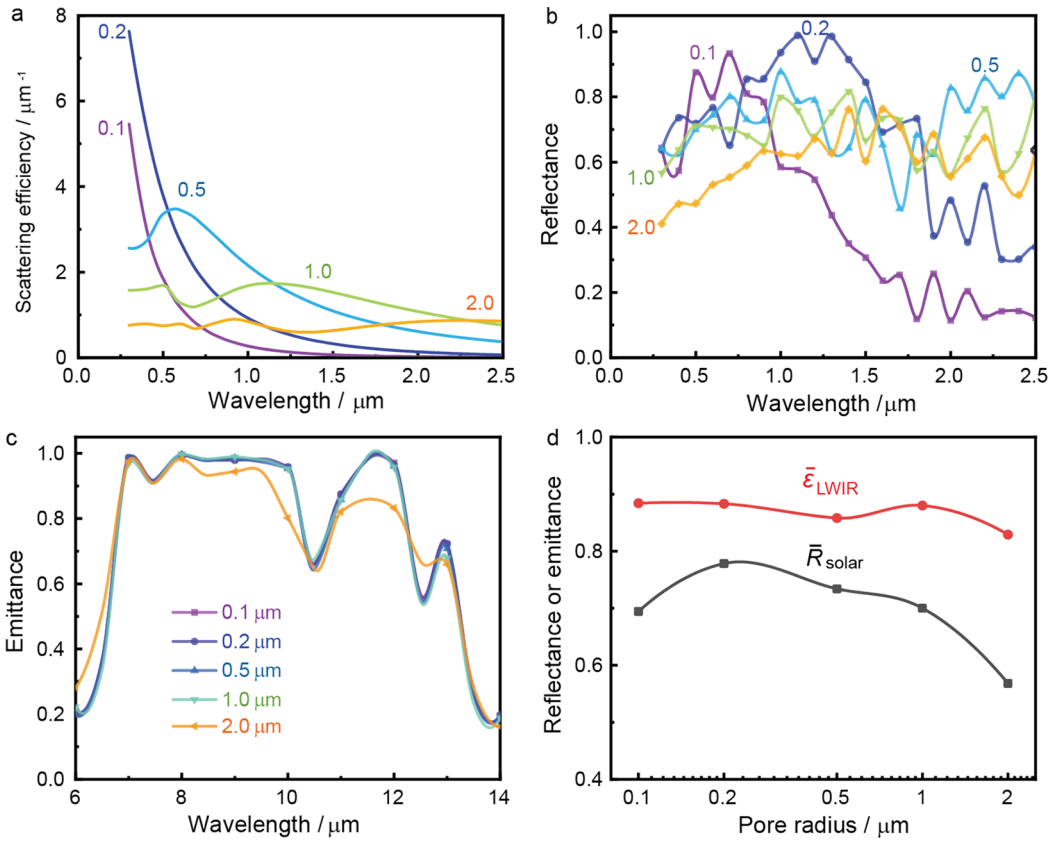

Figure 2. Effects of the pore radius (0.1−2 μm) on $\bar{R}_{solar}$ and $\bar{\varepsilon}_{LWIR}$ of porous P(VdF-HFP) coatings. (a) Simulated scattering efficiency of porous P(VdF-HFP) with different pore radii. (b) Simulated reflectance spectra of a porous coating with different pore radii in the solar spectrum (λ = 0.3−2.5 μm). (c) Simulated emittance spectra of a porous coating with different pore radii in the mid-infrared region (λ = 6.0−14 μm). (d) Calculated $\bar{R}_{solar}$ and $\bar{\varepsilon}_{LWIR}$ with different pore radii. The coating porosity and the thickness are 0.5 and 100 μm, respectively. In (a) and (b), the number next to curves is the corresponding pore radius in micrometers (μm).

In the 2D simulation, we first optimize simulation parameters to realize a balance between accuracy and computational load (Figure S4 and Section 2 in the Supporting Information). For example, a maximum mesh size of 30 nm and a width of 15 μm are chosen for all simulations, which produces reasonable agreement with 3D experimental results in the literature. For instance, the simulated transmittance spectra at 93 μm (Figure 1b) and reflectance spectra at 300 μm (Figure 1c) agree well with experimental data in ref 20. Moreover, as the mismatch mainly occurs in regions with low solar flux (1.2−2.5 μm) and mild radiation (13−14 μm), and the difference between experiment and simulation partially cancels out, the differences in spectrum-averaged $\bar{R}_{solar}$ and $\bar{\varepsilon}_{LWIR}$ are small (0.96 vs 0.91 and 0.97 vs 0.92). Such consistency is further confirmed by the case with monodispersed pore sizes, where the simulated porous structure resembles the experiments better (Figure S5). The differences between the simulation and experiment in $\bar{R}_{solar}$ and $\bar{\varepsilon}_{LWIR}$ are less than 0.02 (0.46 vs 0.45 and 0.93 vs 0.95). These results indicate that our 2D model is effective to evaluate radiative cooling performance. Moreover, as this work only tries to understand the optimal geometry (e.g., pore sizes, porosity) for radiative cooling, but not predict the exact optical spectra, systematic shifts in R and ε should have little effect on the conclusion. However, it should be noted that with 2D simulation it is difficult to obtain precise optical spectra of 3D structures. Further investigations, such as new algorithms, may help compute 3D structures more efficiently with more accurate results.

Figure 1c shows that a thickness of ~300 μm is needed to render high $\bar{R}_{solar}$. However, such thickness is very expensive in computation, especially with varying multiple parameters, as discussed below. Since $\bar{R}_{solar}$ and $\bar{\varepsilon}_{LWIR}$ increase monotonously with thickness, we will first use a thickness of 100 μm as a baseline to understand the effects of different parameters (e.g., pore radius, porosity), followed by evaluating the performance at 300 μm with optimized pore structures.

Effects of Pore Radius on Optical Properties. The classic Mie scattering theory shows that the scattering efficiency of a single pore strongly depends on r.[30] Figure 2a shows that in porous P(VdF-HFP), the scattering peak is red-shift with increasing r, and the maximum scattering efficiency occurs at a wavelength slightly larger than r. For the band with the highest solar flux (e.g., 0.4−0.7 μm), pores with an r value in the range of 0.1−0.5 μm show the strongest scattering efficiency.

After pores with different r are incorporated into a P(VdF-HFP) slab, these porous structures' reflectance spectra show a trend relevant, but distinctly different from, the scattering efficiency, since R depends on both r and the pore density. For example, the scattering efficiency monotonically decreases for r = 0.1 μm. In contrast, nanopores with r = 0.1 μm show a high R of 0.58−0.93 for λ = 0.4−1.0 μm, followed by decreasing to ~0.1 for λ = 1.5−2.5 μm (Figure 2b), at a fixed porosity (ρ) of 0.5. As sunlight concentrates in the range of λ = 0.4−1 μm,

https://dx.doi.org/10.1021/acs.nanolett.0c04241
Nano Lett. XXXX, XXX, XXX−XXX

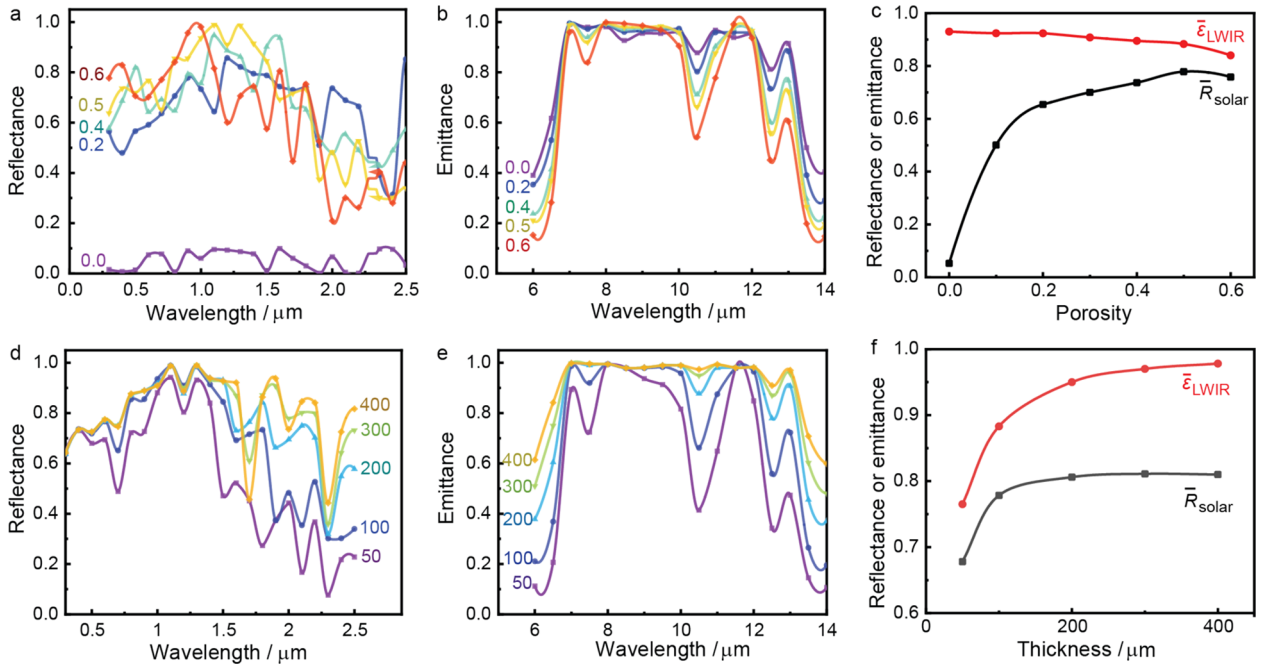

Figure 3. (a–c) Effects of porosity (ρ = 0–0.6) on $\bar{R}_{solar}$ and $\bar{\varepsilon}_{LWIR}$ in porous P(VdF-HFP) coatings. (a) Simulated reflectance spectra of porous coatings with different ρ in the solar spectrum (λ = 0.3–2.5 μm). (b) Simulated emittance spectra of porous coatings with different ρ in the infrared region (λ = 6.0–14 μm). (c) Calculated $\bar{R}_{solar}$ and $\bar{\varepsilon}_{LWIR}$ with different pore radii. The r value is 0.2 μm and the t value is 100 μm in all cases of (a) to (c). In (a) and (b), the number next to the curves is the corresponding ρ. (d–f) Effects of the thickness (t) on $\bar{R}_{solar}$ and $\bar{\varepsilon}_{LWIR}$ in P(VdF-HFP) coatings. (d) Simulated reflectance spectra of porous coatings with different t in the solar spectrum (λ = 0.3–2.5 μm). (e) Simulated emittance spectra of the porous coating with different t in the infrared region (λ = 6.0–14 μm). (f) Calculated $\bar{R}_{solar}$ and $\bar{\varepsilon}_{LWIR}$ with different t. The r value is 0.2 μm and the ρ value is 0.5 in all cases of (d) to (f). The number next to the curves in (d) and (e) is the corresponding t in micrometers (μm).

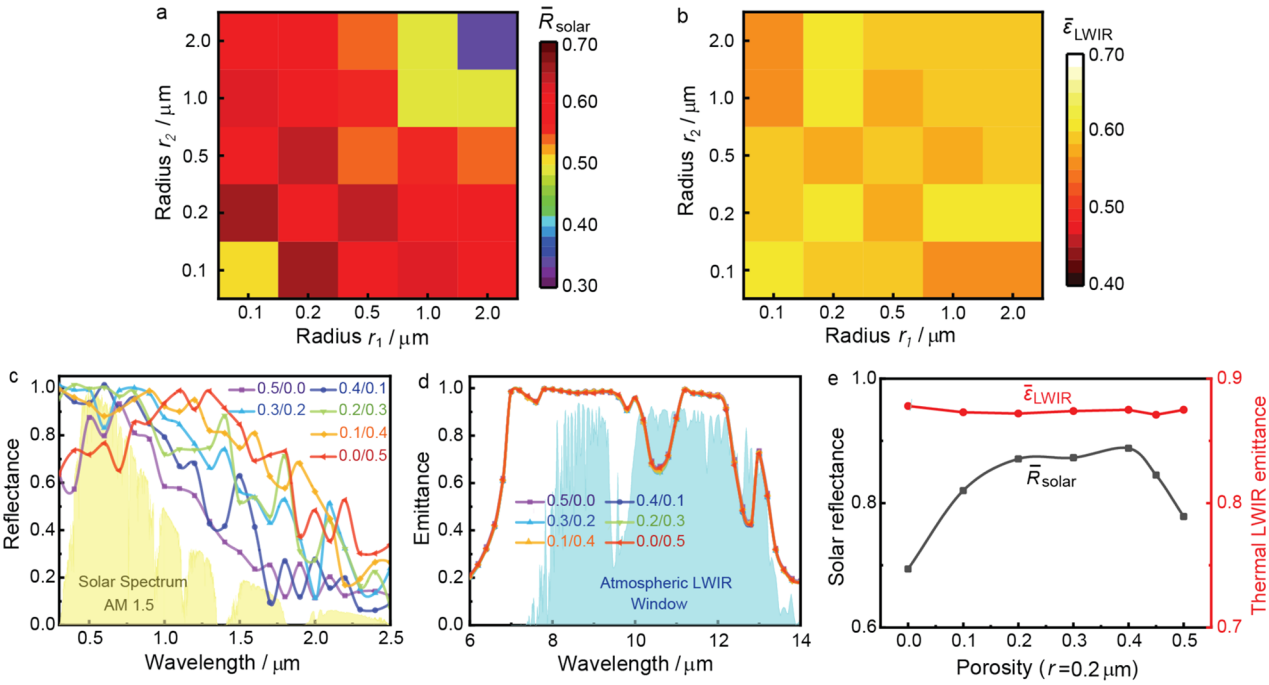

Figure 4. Effect of the pore radius distribution on the cooling performance. (a, b) Maximum (a) $\bar{R}_{solar}$ and (b) corresponding $\bar{\varepsilon}_{LWIR}$ for the porous P(VdF-HFP) coating at different combinations of bimodal pores with two different radii. The coating thickness is 25 μm and the total porosity is 0.5 for all cases of (a) and (b). (c–e) Effects of $\rho_{0.1}$ and $\rho_{0.2}$ on (c) the reflectance spectra in the solar spectrum (λ = 0.3–2.5 μm) and (d) the emittance spectra (λ = 6–14 μm) of porous P(VdF-HFP) coatings. (e) Calculated $\bar{R}_{solar}$ and $\bar{\varepsilon}_{LWIR}$ at different $\rho_{0.2}$. In all cases of (c) to (e), t = 100 μm and $\rho_{r_1} + \rho_{r_2} = 0.5$.

$\bar{R}_{solar}$ increases from 0.694 at r = 0.1 μm to 0.778 at r = 0.2 μm and gradually decreases to 0.734 at r = 0.5 μm and 0.568 at r = 2 μm (Figures 2b and 2d). Therefore, the pore density is as important as the scattering efficiency of a single pore for $\bar{R}_{solar}$. On the other side, $\bar{\varepsilon}_{LWIR}$ does not show a strong dependence on r, as the r value studied is much smaller than the

https://dx.doi.org/10.1021/acs.nanolett.0c04241
Nano Lett. XXXX, XXX, XXX–XXX

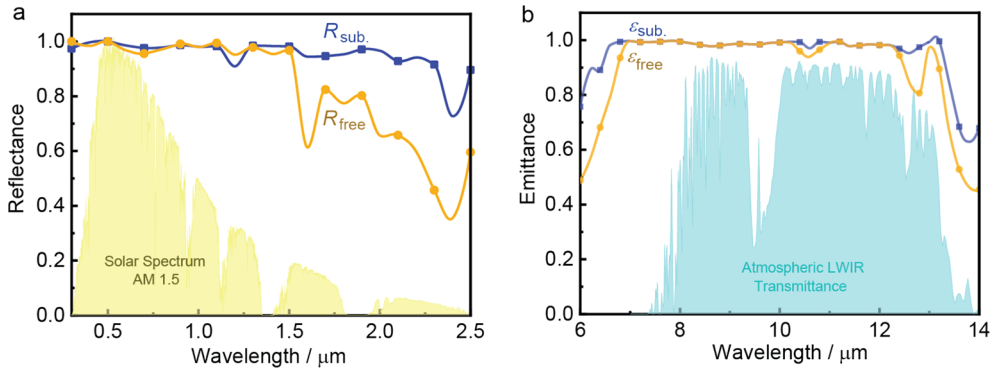

Figure 5. (a) Simulated reflectance and (b) emittance spectra of porous P(VdF-HF) coatings with a substrate (subscript: sub) and without an Al substrate (subscript: free). Mixed pores with r_1 = 0.1 μm and r_2 = 0.2 μm at $\rho_{0.1}$ = 0.1 and $\rho_{0.2}$ = 0.4 are used. In both cases, t = 300 μm. For the case without a substrate, we use absorption to represent emittance to be conservative in reported values.

corresponding wavelength (8−13 μm, Figures 2c and 2d), such that the mesoporous structure can be treated as an effective media. Since P(VdF-HFP) is highly absorptive in the LWIR window, $\overline{\varepsilon}_{LWIR}$ is close to 0.9 for all r. Hence, the pore radius is optimized to 0.2 μm to enhance $\overline{R}_{solar}$ while maintaining a high $\overline{\varepsilon}_{LWIR}$.

Effects of Porosity and Thickness on Optical Properties. Porosity (ρ) is another critical parameter for PDRC performance. To study the effect of porosity, we fix r as 0.2 μm and the thickness as 100 μm. With increasing ρ from 0 to 0.6, more pores exist to scatter sunlight, resulting in enhanced $\overline{R}_{solar}$ (Figures 3a and 3c). $\overline{R}_{solar}$ increases from 0.053 at ρ = 0 to 0.501 at ρ = 0.1 and to 0.778 at ρ = 0.5, followed by decreasing slightly to 0.758 at ρ = 0.6. Such reduction is likely due to the enhanced transmittance with a larger porosity. On the other side, a higher ρ reduces the fraction of polymer, weakening absorptance (i.e., emittance) in the mid-infrared region (Figures 3b and 3c). Hence, $\overline{\varepsilon}_{LWIR}$ decreases gradually from 0.930 to 0.840 when ρ increases from 0 to 0.6, which further confirms that $\overline{\varepsilon}_{LWIR}$ is mainly determined by the effective thickness (= $(1-\rho)t$) of the coating. Therefore, to balance $\overline{R}_{solar}$ and $\overline{\varepsilon}_{LWIR}$, the porosity ρ is set to 0.5 to maximize $\overline{R}_{solar}$ while decreasing $\overline{\varepsilon}_{LWIR}$ only slightly.

Regarding thickness (t), incident photons travel longer in the porous structure in a thicker coating, which would enhance the probability of scattering by pores, resulting in a higher $\overline{R}_{solar}$. A larger t would further increase the effective thickness of bulk polymer, leading to enhanced $\overline{\varepsilon}_{LWIR}$. However, this is at the expense of more materials, so it is important to discover a suitable thickness that balances PDRC performance and material cost.

We use the optimal r and ρ above (0.2 μm and 0.5) for understanding the effect of t (Figures 3d to 3f). $\overline{R}_{solar}$ increases quickly from 0.678 to 0.806 when t increases from 50 to 200 μm, and then, it saturates at 0.810 once t reaches 400 μm. On the other side, $\overline{\varepsilon}_{LWIR}$ increases quickly from 0.765 at t = 50 μm to 0.950 at t = 200 μm, followed by gradual increase to 0.970 at t = 300 μm and 0.976 at t = 400 μm. Therefore, to balance the cooling performance and material cost, a t value of ∼200−300 μm is best, consistent with previous experimental results.[20]

Effect of Pore Radius Distribution on the Cooling Performance. The studies above focus on a single pore radius, but nonuniform pore radii may further enhance performance. Unfortunately, size distribution is of infinite dimension since size can vary continuously. To simplify the problem, we only consider bimodal here as an example. The porosities of two kinds of pores with different radii (r_1, r_2) are denoted as ρ_{r_1} and ρ_{r_2}, respectively, and $\rho_{r_1} + \rho_{r_2}$ is fixed as 0.5. To reduce the computational load, the coating thickness is set to 25 μm, since computations of different ρ_{r_1}/ρ_{r_2} combinations are needed for each r_1/r_2 pair.

Figures 4a and 4b show the effect of (r_1, r_2) on $\overline{R}_{solar}$ and $\overline{\varepsilon}_{LWIR}$, respectively. In each r_1/r_2 combination, results from the optimal ρ_{r_1}/ρ_{r_2} are presented (Table S1). In Figure 4a, the highest $\overline{R}_{solar}$ is 0.657 when $\rho_{0.1}$ = 0.1 and $\rho_{0.2}$ = 0.4 (the unit of micrometers is removed in all subscripts). The second highest value (0.644) occurs for $\rho_{0.2}$ = 0.4 and $\rho_{0.5}$ = 0.1. These results echo with Figure 2, where the highest $\overline{R}_{solar}$ occurs at r = 0.1−0.5 μm. However, the $\overline{R}_{solar}$ of 0.657 is 7.2% higher than the maximum value with single-sized pores ($\overline{R}_{solar}$ = 0.613 at r = 0.2 μm). This is because nanopores with r = 0.2 μm give the highest R (∼0.91−0.94) in λ = 1.0−1.4 μm, but R in the visible spectrum is smaller (∼0.64−0.77). Hence, the addition of smaller nanopores (r = 0.1 μm) can effectively scatter and reflect visible light, thus enhancing $\overline{R}_{solar}$. Figure 4a also shows that $\overline{R}_{solar}$ of a combination of micropores and nanopores (e.g., 0.584 at r_1/r_2 = 2/0.1 μm) is only slightly smaller than the optimal condition (0.657 at r_1/r_2 = 0.2/0.1 μm), indicating that the pore structure in our previous work[20] is near optimal. On the other side, $\overline{\varepsilon}_{LWIR}$ shows a much weaker dependence on the distribution of pore radius, which are all between 0.554 and 0.604 (Figure 4b). These results demonstrate that having a broader size distribution can help enhance $\overline{R}_{solar}$, the optimal radii are 0.1−0.5 μm, and a bimodal of micro- and nanopores are also effective to reflect sunlight.

To further understand how blended mesopores affect optical properties, we study the optical spectra at different ρ_{r_1}/ρ_{r_2} under the optimal conditions (r_1/r_2 = 0.2/0.1 μm) and t = 100 μm (Figures 4c to 4e). In the ultraviolet region (λ = 0.3−0.4 μm), a single r of 0.1 or 0.2 μm results in a small R of 0.6−0.7, but blended pores greatly enhance R due to the interaction of different pores in the mesoporous structure under dependent scattering condition.[31,32] In the near-infrared region of λ ∼ 1.5−2.5 μm, R decreases with increasing $\rho_{0.1}$ due to the different scattering ability of pores with r = 0.1 and 0.2 μm in Figure 2a. Hence, the reflectance spectrum is optimized at $\rho_{0.1}/\rho_{0.2}$ = 0.1/0.4 for $\overline{R}_{solar}$ (Figure 4c).

On the other side, since $\rho_{r_1} + \rho_{r_2}$ is fixed as 0.5, the infrared emittance spectrum is almost identical when ρ_{r_1} and ρ_{r_2} vary and $\overline{\varepsilon}_{LWIR}$ stays at ∼0.87 (Figures 4d and 4e). This agrees well

https://dx.doi.org/10.1021/acs.nanolett.0c04241
Nano Lett. XXXX, XXX, XXX−XXX

with that the emittance is mainly determined by the effective thickness of P(VdF-HFP). In contrast, $\bar{R}_{solar}$ increases gradually from 0.694 to 0.888 when $\rho_{0.2}$ increases from 0 to 0.4, followed by dropping to 0.845 and 0.778 when $\rho_{0.2}$ increases to 0.45 and 0.5, respectively (Figure 4e). Besides the 0.1/0.2 μm case, a similar behavior is also observed with r_1/r_2 of 0.2/0.5 μm (Figure S6).

Although quasi-bimodal pores (r = 0.10 ± 0.09 μm and 2.74 ± 0.71 μm) were demonstrated in the literature,[20] it should be noted that the precise bimodal design may be challenging to fabricate in a scalable and low-cost fashion. The analysis on the bimodal design is to point out that the incorporation of pores with different sizes can help enhance light scattering and $\bar{R}_{solar}$ compared to a single size, and it is optimal to have both pore sizes between 0.1 and 0.5 μm. More discussions are in Section 6 of the Supporting Information.

Net Cooling Power in the Optimized Porous Structure. The analyses above identify mixed nanopores with r_1 = 0.1 μm and r_2 = 0.2 μm at $\rho_{0.1}$ = 0.1 and $\rho_{0.2}$ = 0.4 as the optimal condition. Hence, a substrate-free coating with t = 300 μm and such pore geometry is simulated (yellow lines in Figure 5). The simulated $\bar{R}_{solar}$ and $\bar{\varepsilon}_{LWIR}$ reach 0.951 and 0.969, respectively. Hence, under the standard AM 1.5 solar spectrum and a typical atmospheric condition (semihumid),[33] the radiation power from the coating to the sky is P_{rad} = 249 W/m^2, the solar heating power is P_{sun} = 44 W/m^2, the radiation from the atmosphere to the coating is P_{atm} = 161 W/m^2, and the net cooling power is $P_{cool} = P_{rad} - P_{sun} - P_{atm}$ = 44 W/m^2, when the coating temperature and the ambient temperature are both 25 °C. This is attractive for PRDC, and the value is comparable with previous results.[19] Note that such P_{cool} is a conservative estimation since (1) most common substrates (e.g., metals, concrete, wood) further enhance $\bar{R}_{solar}$ compared to a freestanding film. (2) Absorption is used for calculating emittance, so that $\bar{\varepsilon}_{LWIR}$ is the smallest possible value. The error in the cooling power is estimated to be <5% since R and ε depend on the incident angle θ. Details can be found in Section 7 of the Supporting Information.

R and ε above are conservative estimations as no substrate is used. With an Al substrate under the porous coating above, the substrate further reflects sunlight, and the porous medium can absorb more mid-infrared light. Hence, $\bar{R}_{solar}$ and $\bar{\varepsilon}_{LWIR}$ increase to 0.980 and 0.984, respectively. Under the same atmospheric conditions and solar spectrum discussed above, P_{cool} = 72 W/m^2, which is 79% of an ideal emitter (P_{cool} = 91 W/m^2). Details are provided in Section 7 of the Supporting Information.

CONCLUSION

In summary, we built a simulation model to understand the relationship between geometric properties of a mesoporous coating (e.g., pore radius, porosity, thickness) and its PDRC performance. When single-sized pores are used, the maximum $\bar{R}_{solar}$ is obtained with a nanopore radius of 0.2 μm and porosity of 0.5. On the other side, $\bar{\varepsilon}_{LWIR}$ is mainly determined by the effective total thickness of polymer inside, since the pore radius is much smaller than the infrared wavelength. We also find that a broad pore distribution helps enhance $\bar{R}_{solar}$. In a simplified case, bimodal pores with radii of 0.1 and 0.2 μm lead to a higher $\bar{R}_{solar}$ of 0.951 and $\bar{\varepsilon}_{LWIR}$ of 0.969 at a thickness of 300 μm and porosity of 0.5, which is much larger than the maximum $\bar{R}_{solar}$ of 0.811 with single-sized pores. Hence, the corresponding cooling power is 44 W/m^2 under a semihumid atmospheric condition and the standard AM 1.5 solar spectrum. Moreover, the PDRC performance can be further enhanced by placing an Al substrate underneath, which increases both $\bar{R}_{solar}$ and $\bar{\varepsilon}_{LWIR}$ to 0.98 and renders a high cooling power of 72 W/m^2. This study provides a guide to design the material structure in a porous coating for maximizing PDRC performance.

ASSOCIATED CONTENT

Supporting Information

The Supporting Information is available free of charge at https://pubs.acs.org/doi/10.1021/acs.nanolett.0c04241.

Additional details for the reflectance simulation model; determination of simulation parameters; fabrication and optical properties of porous P(VdF-HFP) coatings with monodiserpsed pores; effects of pore radius distribution on the cooling performance; cooling performance of structures with different pore size distributions; radiative cooling performance of bimodal pore coatings; and calculation of cooling power (PDF)

AUTHOR INFORMATION

Corresponding Author

Yuan Yang − *Program of Materials Science and Engineering, Department of Applied Physics and Applied Mathematics, Columbia University, New York 10027, United States;* orcid.org/0000-0003-0264-2640; Email: yy2664@columbia.edu

Authors

Meijie Chen − *School of Energy Science and Engineering, Central South University, Changsha 410083, China; Program of Materials Science and Engineering, Department of Applied Physics and Applied Mathematics, Columbia University, New York 10027, United States*

Dan Pang − *School of Energy Science and Engineering, Central South University, Changsha 410083, China*

Jyotirmoy Mandal − *Department of Materials Science and Engineering, University of California, Los Angeles, Los Angeles, California 90095, United States;* orcid.org/0000-0001-8124-5234

Xingyu Chen − *School of Energy Science and Engineering, Central South University, Changsha 410083, China*

Hongjie Yan − *School of Energy Science and Engineering, Central South University, Changsha 410083, China*

Yurong He − *School of Energy Science and Engineering, Harbin Institution of Technology, Harbin 180001, China;* orcid.org/0000-0003-3009-0468

Nanfang Yu − *Program of Materials Science and Engineering, Department of Applied Physics and Applied Mathematics, Columbia University, New York 10027, United States*

Complete contact information is available at: https://pubs.acs.org/10.1021/acs.nanolett.0c04241

Notes

The authors declare no competing financial interest.

ACKNOWLEDGMENTS

Y.Y. acknowledges support from the National Science Foundation (award no. 2005747). J.M. was supported by Schmidt Science Fellows, in partnership with the Rhodes

Trust. M.C. would like to acknowledge the support from National Natural Science Foundation of China (52006246).

REFERENCES

(1) Isaac, M.; van Vuuren, D. P. Modeling Global Residential Sector Energy Demand for Heating and Air Conditioning in the Context of Climate Change. *Energy Policy* **2009**, *37* (2), 507−521.
(2) Abberton, M. T. Greenhouse Gas Emissions. *Genomics and Breeding for Climate-Resilient Crops* **2013**, *2*, 457−474.
(3) Steven Brown, J.; Domanski, P. A. Review of Alternative Cooling Technologies. *Appl. Therm. Eng.* **2014**, *64* (1−2), 252−262.
(4) Chen, M.; He, Y.; Hu, Y.; Zhu, J. Journal of Quantitative Spectroscopy & Radiative Transfer Local Temperature Control of Hybrid Plasmonic Nano-Antennas. *J. Quant. Spectrosc. Radiat. Transfer* **2019**, *225*, 50−57.
(5) Levinson, R.; Akbari, H. Potential Benefits of Cool Roofs on Commercial Buildings: Conserving Energy, Saving Money, and Reducing Emission of Greenhouse Gases and Air Pollutants. *Energy Effic.* **2010**, *3* (1), 53−109.
(6) Baniassadi, A.; Sailor, D. J.; Ban-Weiss, G. A. Potential Energy and Climate Benefits of Super-Cool Materials as a Rooftop Strategy. *Urban Clim.* **2019**, *29*, 100495.
(7) Shi, N. N.; Tsai, C. C.; Camino, F.; Bernard, G. D.; Yu, N.; Wehner, R. Keeping Cool: Enhanced Optical Reflection and Radiative Heat Dissipation in Saharan Silver Ants. *Science* **2015**, *349* (6245), 298−301.
(8) Rephaeli, E.; Raman, A.; Fan, S. Ultrabroadband Photonic Structures to Achieve High-Performance Daytime Radiative Cooling. *Nano Lett.* **2013**, *13* (4), 1457−1461.
(9) Zhao, B.; Ao, X.; Chen, N.; Xuan, Q.; Hu, M.; Pei, G. General Strategy of Passive Sub-Ambient Daytime Radiative Cooling. *Sol. Energy Mater. Sol. Cells* **2019**, *199*, 108−113.
(10) Raman, A. P.; Anoma, M. A.; Zhu, L.; Rephaeli, E.; Fan, S. Passive Radiative Cooling below Ambient Air Temperature under Direct Sunlight. *Nature* **2014**, *515* (7528), 540−544.
(11) Zhao, D.; Aili, A.; Zhai, Y.; Lu, J.; Kidd, D.; Tan, G.; Yin, X.; Yang, R. Subambient Cooling of Water: Toward Real-World Applications of Daytime Radiative Cooling. *Joule* **2019**, *3* (1), 111−123.
(12) Gentle, A. R.; Smith, G. B. Radiative Heat Pumping from the Earth Using Surface Phonon Resonant Nanoparticles. *Nano Lett.* **2010**, *10* (2), 373−379.
(13) Kou, J.-l.; Jurado, Z.; Chen, Z.; Fan, S.; Minnich, A. J. Daytime Radiative Cooling Using Near-Black Infrared Emitters. *ACS Photonics* **2017**, *4* (3), 626−630.
(14) Zhao, D.; Aili, A.; Zhai, Y.; Xu, S.; Tan, G.; Yin, X.; Yang, R. Radiative Sky Cooling: Fundamental Principles, Materials, and Applications. *Appl. Phys. Rev.* **2019**, *6*, 1.
(15) Wang, X.; Liu, X.; Li, Z.; Zhang, H.; Yang, Z.; Zhou, H.; Fan, T. Scalable Flexible Hybrid Membranes with Photonic Structures for Daytime Radiative Cooling. *Adv. Funct. Mater.* **2020**, *30* (5), 1907562.
(16) Zhou, L.; Song, H.; Liang, J.; Singer, M.; Zhou, M.; Stegenburgs, E.; Zhang, N.; Xu, C.; Ng, T.; Yu, Z.; Ooi, B.; Gan, Q. A Polydimethylsiloxane-Coated Metal Structure for All-Day Radiative Cooling. *Nat. Sustain.* **2019**, *2* (8), 718−724.
(17) Yang, Y.; Zhang, Y. Passive Daytime Radiative Cooling: Principle, Application, and Economic Analysis. *MRS Energy Sustain.* **2020**, *7*, 1−8.
(18) Zhao, B.; Hu, M.; Ao, X.; Chen, N.; Pei, G. Radiative Cooling: A Review of Fundamentals, Materials, Applications, and Prospects. *Appl. Energy* **2019**, *236*, 489−513.
(19) Zhai, Y.; Ma, Y.; David, S. N.; Zhao, D.; Lou, R.; Tan, G.; Yang, R.; Yin, X. Scalable-Manufactured Randomized Glass-Polymer Hybrid Metamaterial for Daytime Radiative Cooling. *Science* **2017**, *355* (6329), 1062−1066.
(20) Mandal, J.; Fu, Y.; Overvig, A. C.; Jia, M.; Sun, K.; Shi, N. N.; Zhou, H.; Xiao, X.; Yu, N.; Yang, Y. Hierarchically Porous Polymer Coatings for Highly Efficient Passive Daytime Radiative Cooling. *Science* **2018**, *362* (6412), 315−319.
(21) Mandal, J.; Yang, Y.; Yu, N.; Raman, A. P. Paints as a Scalable and Effective Radiative Cooling Technology for Buildings. *Joule* **2020**, *4* (7), 1350−1356.
(22) Chen, Y.; Mandal, J.; Li, W.; Smith-Washington, A.; Tsai, C. C.; Huang, W.; Shrestha, S.; Yu, N.; Han, R. P. S.; Cao, A.; Yang, Y. Colored and Paintable Bilayer Coatings with High Solar-Infrared Reflectance for Efficient Cooling. *Sci. Adv.* **2020**, *6* (17), eaaz5413.
(23) Mandal, J.; Jia, M.; Overvig, A.; Fu, Y.; Che, E.; Yu, N.; Yang, Y. Porous Polymers with Switchable Optical Transmittance for Optical and Thermal Regulation. *Joule* **2019**, *3* (12), 3088−3099.
(24) Peng, Y.; Chen, J.; Song, A. Y.; Catrysse, P. B.; Hsu, P. C.; Cai, L.; Liu, B.; Zhu, Y.; Zhou, G.; Wu, D. S.; Lee, H. R.; Fan, S.; Cui, Y. Nanoporous Polyethylene Microfibres for Large-Scale Radiative Cooling Fabric. *Nat. Sustain.* **2018**, *1* (2), 105−112.
(25) Torgerson, E.; Hellhake, J. Polymer Solar Filter for Enabling Direct Daytime Radiative Cooling. *Sol. Energy Mater. Sol. Cells* **2020**, *206*, 110319.
(26) Li, D.; Liu, X.; Li, W.; Lin, Z.; Zhu, B.; Li, Z.; Li, J.; Li, B.; Fan, S.; Xie, J.; Zhu, J. Scalable and Hierarchically Designed Polymer Film as a Selective Thermal Emitter for High-Performance All-Day Radiative Cooling. *Nat. Nanotechnol.* **2020**, 1−6.
(27) Li, T.; Zhai, Y.; He, S.; Gan, W.; Wei, Z.; Heidarinejad, M.; Dalgo, D.; Mi, R.; Zhao, X.; Song, J.; Dai, J.; Chen, C.; Aili, A.; Vellore, A.; Martini, A.; Yang, R.; Srebric, J.; Yin, X.; Hu, L. A Radiative Cooling Structural Material. *Science* **2019**, *364* (6442), 760−763.
(28) Aili, A.; Wei, Z. Y.; Chen, Y. Z.; Zhao, D. L.; Yang, R. G.; Yin, X. B. Selection of Polymers with Functional Groups for Daytime Radiative Cooling. *Mater. Today Phys.* **2019**, *10*, 100127.
(29) Bella, F.; Griffini, G.; Correa-Baena, J. P.; Saracco, G.; Grätzel, M.; Hagfeldt, A.; Turri, S.; Gerbaldi, C. Improving Efficiency and Stability of Perovskite Solar Cells with Photocurable Fluoropolymers. *Science* **2016**, *354* (6309), 203−206.
(30) Chen, M.; Yan, H.; Zhou, P.; Chen, X. Transparent Display by the Scattering Effect of Plasmonic Au-Ag Nanoparticles. *Plasmonics* **2020**, *15* (6), 1855−1861.
(31) Ma, L. X.; Wang, C. C.; Tan, J. Y. Light Scattering by Densely Packed Optically Soft Particle Systems, with Consideration of the Particle Agglomeration and Dependent Scattering. *Appl. Opt.* **2019**, *58* (27), 7336.
(32) Drolen, B. L.; Tien, C. L. Independent and Dependent Scattering in Packed-Sphere Systems. *J. Thermophys. Heat Transfer* **1987**, *1* (1), 63−68.
(33) Berk, A.; Conforti, P.; Kennett, R.; Perkins, T.; Hawes, F.; van den Bosch, J. MODTRAN6: A Major Upgrade of the MODTRAN Radiative Transfer Code. *Proc. SPIE* **2014**, *9088*, 90880H.

https://dx.doi.org/10.1021/acs.nanolett.0c04241
Nano Lett. XXXX, XXX, XXX−XXX